Study of sea-ice pressure ridge distributions from in-situ laser profiler measurements and ERS SAR signatures

Liu, Q., C. Haas, T. Martin, and E. Augstein
Alfred Wegener Institute for Polar and Marine Research, Am Handelshafen 12, 27570 Bremerhaven, F. R. Germany

1 Introduction

Sea-ice pressure ridges are primarily generated when ice motion converges and floes are compressed. Along adjacent floe edges ice blocks form ridges above and keels below the water level (**Fig. 1**). The magnitude of deformation depends on the atmospheric and/or oceanic forces [1]. In numerical sea-ice models [2] ice deformation is treated by certain rheology concepts which have to be validated by observations.

This requirement has to be met with high temporal and spatial resolution. In particular the Synthetic Aperture Radar (SAR) onboard ERS-1 and ERS-2 can resolve rather small horizontal scales and is able to detect features like ice ridges. The ice of pressure ridges has a lower density and a higher porosity than the surrounding level ice. Furthermore some surfaces of the ice blocks are oriented almost normal to the incident radar rays, ranging from 20 to 26° elevation. Consequently, the backscatter power of ridges is distinctly larger than that of level ice [3]. Therefore, the spatial density of pressure ridges is to a certain extent reflected in the backscatter signal of the SAR [3], [4]. And in fact ridges are obvious as black lines of higher backscatter power on floes with diameters beyond a couple of hundred meters on an ERS SAR images from the Arctic Ocean (**Fig. 2**). If the ice cover consists mainly of rather small floes like on the image from the Weddell Sea (**Fig. 3**), ridges are not as clearly visible. However, leads and ice are clearly distinguishable. Unfortunately, there is no unique relationship between the SAR backscatter coefficients and the ice roughness. Therefore, special efforts are required to derive the statistical distribution of pressure ridges from ERS SAR data for defined areas. Subsequently, here we are proposing a

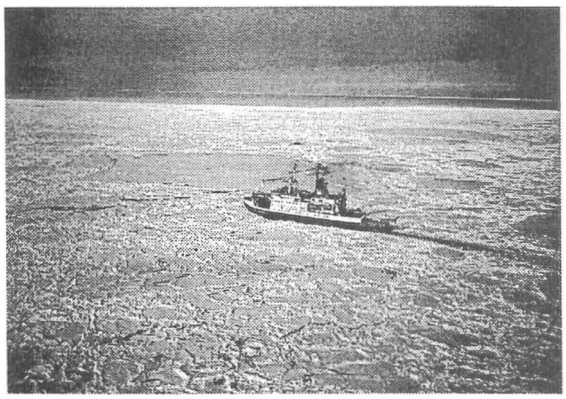

Fig. 1 Photograph showing the German research icebreaker POLARSTERN passing thruogh the ice, taken from a helicopter at a height of approx. 50 m in February 1997 in the Weddell Sea. The ice surface consists of alternating pressure ridges and level areas.

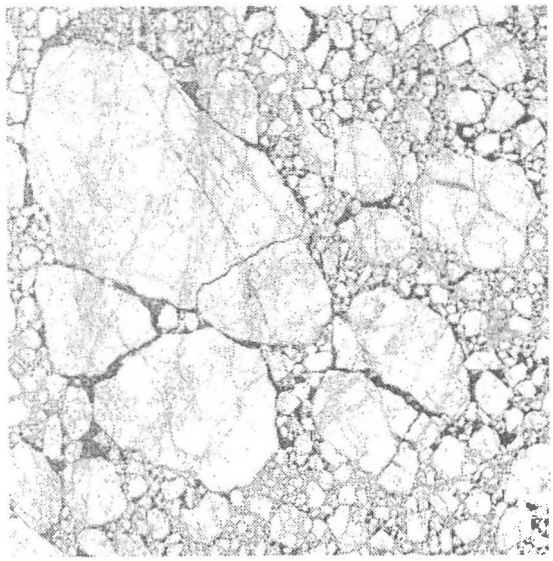

Fig. 2 Section (40 km x 40 km) of an ERS SAR scene from August 3 1996 (orbit 6732, frame 1827). Dark greytones represent large backscatter coefficients.

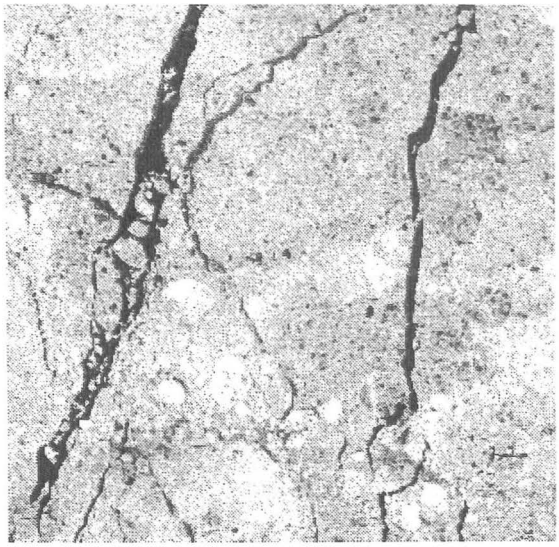

Fig. 3 Section (40 km x 40 km) of an ERS SAR scene from March 1 1997 (orbit 9738, frame 5139). Dark greytones represent large backscatter coefficients.

method based on a neural network. The scheme is applied for perennial Antarctic ice in summer when helicopterborne laser profiler measurements could be carried out for ground truthing.

2 Methods and measurements

Comprehensive laser profiler measurements were performed in the Bellingshausen and Amundsen Seas in February 1994 and in the Weddell Sea in February 1997 by means of helicopter along flight tracks of more than 100 km length each. These measurements yielded information on the surface morphology, in particular the height of and spacing between pressure ridges (see e.g [5]). Several flights were performed within the footprint of the ERS SAR. The time of the SAR overflights was almost simultaneous, or differed only a few days from the helicopter flights. Together, 14 flights were carried out with coincident SAR images available. The images were calibrated according to [6]. Then, the original resolution of 12.5 m was reduced to a resolution of 100 m by averaging 8x8 pixels to eliminate speckle and noise in the image. The SAR backscatter coefficients are mainly dependent on the roughness, thickness, and salinity of the ice. Therefore, to extract a single property, more information than the single backscatter coefficient at 5.3 GHz and vertical polarization is needed. A reasonable attempt is made in using the mean value, the variance and the half-width of the distribution of backscatter coefficients from an area of about 50 km by 50 km. The three variables form the input for a retrieving algorithm, which is based on a neural network. As the relationship between the moments of the distribution and the mean ridge spacing is not linear, a neural network approach is superior to a linear regression method [7]. Here, we use a layered perceptron-type artificial neural network [8]. It has one input layer, one hidden layer, and one output layer. Each layer employs one or more neurons and each neuron in the same layer is connected with different weights to the adjacent layer. The weights can be calculated from a backpropagation learning algorithm based on a training dataset. This backpropagation algorithm uses the gradient descent method to get a local minimum between the calculated output and the actual output. The rms error of the neural network for retrieving the spacing of pressure ridges is about 1/3 of that by using the regression method. The neural network algorithm is trained with the ground truth and SAR data from the Bellingshausen and Amundsen Seas, and then applied to the Weddell Sea SAR data.

3 Results

From the laser measurements, a strong contrast in spatial ridge density (or mean ridge spacing, respectively) was found for two flights in the Bellingshausen and Amundsen Sea. The ice in the central Bellingshausen Sea was only moderately deformed. The average ridge height and the average spacing between ridges (cut-off height 0.8 m) were found to be 1.08 m and 321 m, respectively (**Fig. 4**). In the eastern Amundsen Sea, up to 50% of the floe surface was deformed. The mean ridge height and spacing were 1.16 m and 63 m (see **Fig. 4**), respectively. Thus, for both regions the average height difference of the ridges is small, but the average spatial density is quite different. As shown in **Fig. 4**, in the Amundsen Sea ridge spacings between 0 and 100 m occur about twice as often as in the Bellingshausen Sea. A significant difference can also be seen in the nearly simultaneous SAR scenes (**Fig. 5**), in which a rectangular area of the SAR image matching the laser profiler tracks was selected. Mean values of -7.64 dB are derived for the Bellingshausen Sea

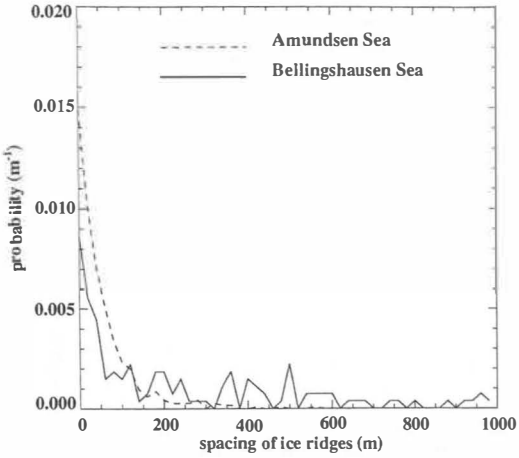

Fig. 4 Probability density of pressure ridges in the Bellingshausen and Amundsen Seas, measured with the laser profiler.

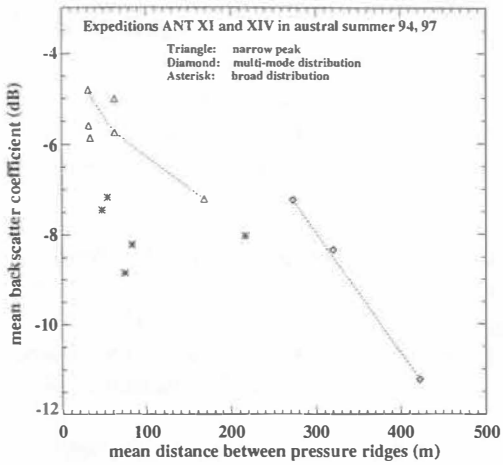

Fig. 6 Mean distance between ridges derived from laser profiler measurements versus mean backscatter coefficients from coincident ERS SAR images

and of -5.01 dB for the highly deformed ice in the Amundsen Sea. The distributions of SAR backscatter coefficients in the Bellingshausen and Amundsen Seas (**Fig. 5**) represent significantly different sea-ice regimes. In the Amundsen Sea, the sea-ice appears relatively homogeneous, which leads to a narrow distribution of the SAR backscatter coefficients. In contrast, the distribution of the backscatter coefficients in the Bellingshausen Sea is multi-modal, resulting from alternating level floes and floes with ridges. Close to the Antarctic Peninsula, the distribution was found to be very wide due to the occurence of a mixture of water, thin ice, as well as level and deformed floes. The backscatter distributions of all processed images could be assigned to one of these classes, namely narrow, multi-mode, and broad distributions (**Fig. 5**).

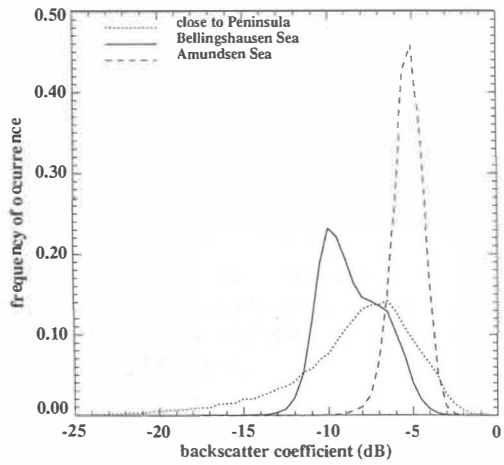

Fig. 5 Histogram of ERS SAR backscatter coefficients for different ice regimes.

Figure 6 shows the relationship between mean ridge spacings derived from all 14 laser measurements and the mean backscatter coefficients of the coincident SAR sub-scene. It can be seen that for the cases of narrow and multi-mode distributions are characterized by decreasing backscatter coefficients with increasing mean distance between ridges. But, there is no clear relationship for the case of the broad distributions. Here we find an ambiguity between ridge spacing and SAR backscatter. Therefore, we apply all of the three aforementioned informations on the backscatter to neural network which is trained with the data from the Bellingshausen and Amundsen Seas. The trained network is applied to the Weddell Sea data from 1997 (**Fig. 7**). With this method a good agreement is achieved between the laser measurements and the retrievals from ERS SAR for the ridge density. The bias between retrievals and measurements is very small [see **Fig. 7**]. The rms error is about 20%, which is sufficient for the purpose of this study. In particular, the large differences between the central Weddell Sea and the northwestern and southeastern Weddell Sea, respectively, are clearly resolved with mean spacings of 220 m for the first and of 32 m for the latter (**Fig. 7**).

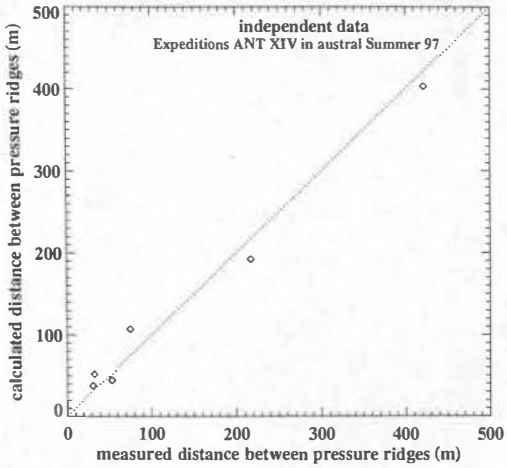

Fig. 7 Comparison of the mean distance between ridges from laser measurements in the Weddell Sea and retrievals from ERS SAR images by means of the neural network.

4 Conclusion

We have developed a neural network scheme which enable us to derive the spacing of the pressure ridges from ERS SAR backscatter information. However, we must admit that more comparisons with in-situ measurements are required to confirm our results. In addition, a powerful surface scattering model is required to investigate the physical processes involved in backscattering from geometric roughness features. Information on ice types may also improve the results of the neural network. The latter may be obtained by means of segmentation algorithms [9].

Acknowledgement

Funding by the German Federal Ministry of Education Research and Technology under the project "Remote Sensing of Sea Ice Characteristics and Processes" (Proj. No. 03PL018B) is gratefully acknowledged. We thank ESA for providing ERS SAR images for this study (project AO2.D146-9).

References

[1] Kottmeier, C. and L. Sellmann, 1996: Atmospheric and oceanic forcing of Weddell Sea ice motion. J. Geophys. Res., 101, C9, 20809-20824.

[2] Harder, M., and P. Lemke, 1994: Modelling the extent of sea ice ridging in the Weddell Sea, In: The polar oceans and their role in shaping the global environment, Geophysical Monograph 85, AGU, Washington, USA.

[3] Johansson, R., and J. Askne, 1987: Modelling of radar backscattering from low-salinity ice with ice ridges. Int. J. Remote Sensing, vol. 8, no. 11, 1667-1677.

[4] Carlström, A., and L. M. H. Ulander, 1995: Validation of backscatter models for level and deformed sea-ice in ERS-1 SAR images. Int. J. Remote Sensing, 16, 3245-3266.

[5] Dierking, W., 1995: Laser profiling of the ice surface topography during the winter Weddell Gyre study. J. Geophys. Res., 100, C3, 4807-4820.

[6] Laur, H., P. Bally, P. Meadows, J. Sanchez, B. Schaettler, and E. Lopinto, 1995: Derivation of the backscattering coefficient σ° in ESA ERS-1/2 SAR.PRI data products. Techical Note, Issue 2, Rev. 1, ESA-ESRIN, pp 42.

[7] Chen, K. S., W. L. Kao, and Y. C. Tzeng, 1995: Retrieval of surface parameters using dynamic learning neural network, Int. J. Remote Sens., 16, 801-809.

[8] Liu, Q., C. Simmer, and E. Ruprecht, 1997: Estimating longwave net radiation at sea surface from the Special Sensor Microwave/Imager (SSM/I), J. Appl. Meteorol., 36, 919-930.

[9] Skriver, H., 1989: Determination of sea ice parameters from SAR data. Proceedings 9th EARSel Symposium, 143-148.